Materials Letters 246 (2019) 17–19

Contents lists available at ScienceDirect

Materials Letters

journal homepage: www.elsevier.com/locate/mlblue

Ytterbium silicide nanostructures prepared by pulsed laser ablation in oven: Structural and electrical characterization

Vladislav Dřínek [a,*], Zdeněk Remeš [b], Mariana Klementová [b], Lukáš Palatinus [b], Markéta Jarošová [b], Alois Lugstein [c], Masiar Sistani [c], Martin Koštejn [a], Věra Jandová [a], Radek Fajgar [a]

[a] Institute of Chemical Process Fundamentals of the CAS, v. v. i., Rozvojová 2/135, 165 02 Prague 6 – Suchdol, Czech Republic
[b] Institute of Physics of the CAS, v.v.i., Na Slovance 2, 182 21 Prague, Czech Republic
[c] Institute for Solid State Electronics, Vienna University of Technology, Floragasse 7, 1040 Vienna, Austria

ARTICLE INFO

Article history:
Received 28 January 2019
Received in revised form 7 March 2019
Accepted 8 March 2019
Available online 13 March 2019

Keywords:
Metals and alloys
Particles
Nanosize
Nanowire
Silicide
Ytterbium

ABSTRACT

Ytterbium silicide nanoobjects were synthetized using pulsed laser ablation in an oven at temperatures of 800 and 1000 °C. Ablation of divided target Si/Yb in a flow of Ar resulted in deposits which contained mostly ytterbium silicide nanowires, nanorods and nanoparticles. Single nanoparticles (800 °C) are identical with Yb_3Si_5 alloy; nanorods possess both a monoclinic phase not corresponding to any known structure in the phase diagram Yb-Si and a face-centered cubic structure close to the pure Yb but with a high Si content. At the temperature of 1000 °C, the studied nanorods and nanowires decorated by nanocrystals are practically amorphous, whereas the structure of those nanocrystals is close to that of the nanorods with the face-centered cubic structure prepared at 800 °C. Nanowire (1000 °C) is a semiconductor with $\rho = 132.9\ \Omega.cm$ at room temperature, which is comparable to a heavily doped silicon.

1. Introduction

Metal silicides are attractive materials due to their property tailoring. By changing the metal concentration and reducing dimensions to nanoscale, the silicide behavior varies from that of a semiconductor to metal, which is an interesting phenomenon for advanced technologies. Silicide compatibility with the current silicon technology is also of advantage.

Ytterbium silicide is an alloy has not yet been studied extensively [1] since scientific interest has focused on more earth abundant metal elements. The thermal behavior of Yb-Si(1 1 1) structure was studied in the temperature range of 300–1500 K [2]. An $YbSi_2$ film was formed at a relatively low temperature despite the fact that the Si-Si bond in bulk silicon is stronger than the Yb-Si bond. The mechanism of this phenomenon was provided. $YbSi_x$ was studied as a stabilizing alloy for $NiSi_x$ metal contacts in electronics [3]. The thermal instability of $NiSi_x$ material at high temperature was reduced in Ta/Ni/Yb stacked layer by the formation of ytterbium silicide which kept the NiSi phase stable in the course of annealing. $YbSi_2$ with a layered structure was also recognized as a promising thermoelectric material with a high power factor and figure of merit at room temperature (RT) [4]. By doping Yb, Yb_3Si_5 inclusions developed in the thermoelectric material Mg_2Si resulting in the decreased bulk thermal conductivity [5].

2. Experimental

Ytterbium silicide deposits were prepared using pulsed laser ablation setup furnished with an oven. First, the quartz tube in the oven was pumped down to 10^{-3} Pa by a turbopump and heated up to the temperature of 800 and 1000 °C. Then, an argon flux of 10 sccm was maintained over polycrystalline silicon substrates in the tube at the pressure of 10 Pa. ArF excimer laser pulses (115 mJ, 10 Hz) were focused by a quartz lens at a two-halves-piece-target made of a polycrystalline silicon sheet and ytterbium (Aldrich, 99.9%) for 15 min.

The morphology of each sample was analysed by a scanning electron microscopy (SEM) setup (TESCAN Vega 3) equipped with an EDX spectrometer (Brukker Detector 5010) for the elemental composition.

The high resolution TEM data collections for the structural investigation and images of samples were recorded on a transmission electron microscope (TEM) with a LaB_6 cathode operating at 120 kV. The microscope was equipped with a DigiStar (NanoMegas)

* Corresponding author.
E-mail address: drinek@icpf.cas.cz (V. Dřínek).

https://doi.org/10.1016/j.matlet.2019.03.032
0167-577X/

precession device, a CCD Camera and EDAX energy dispersive X-ray detector Apollo XLTW.

The diffraction data were collected by means of precession electron diffraction tomography (PEDT). The data were processed with the program PETS [6]. The graphical interface for indexing available in JANA2006 [7] was used to determine the lattice parameters.

For resistivity measurements, the nanowire transfer to the measurement module (p-doped Si substrate with a 100 nm thick, thermally grown SiO_2 layer) was done by the drop-casting method. The devices were prepared by electron beam lithography on a Raith e-LiNE machine (10 kV, PMMA resist) contacting individual NWs. This was followed by a 7 s BHF dip to remove the native oxide shell around the NWs. The contacts were fabricated by the sputter deposition of 7 nm Ti and 150 nm Au. The electrical measurements were performed using a combination of an analyzer (HP 4156B) and a probe station.

3. Results and discussion

Pulsed Laser Deposition (PLD) of an Yb/Si target resulted in the formation of thick black deposits. SEM analysis revealed that the deposits were composed of both nanocrystals/nanopilars/nanoplatelets and nanowires (NWs). For deposits prepared at 800 °C, the nanoobjects were up to 2 μm long and several hundreds nm wide (Fig. S1). The NWs were scarcely scattered among them (Fig. 1a). The overall EDX concentration Si:Yb = 1:0.05 (at. %) was detected in the distance of 4 cm from the target. The elemental mapping (Fig. 1b,c) showed the presence of Si and Yb in the NW material. Yb was inhomogeneously contained due to nanocrystals at the NW surface (see below). Deposits prepared at 1000 °C consisted of both nanocrystals/nanorods/nanoplatelets 4 cm far from the target (Fig. S2) and the NWs 8 cm from the target (Fig. 2d). The NW diameter histogram inset is showed as a part of Fig. 1d. A column represents a count of NWs with the diameter difference of max. 10 nm. The mean value of nanowire diameter was 116 ± 22 nm. A minor maximum is seen for higher diameter values, which can be explained by the formation of different cluster sizes both in silicon and ytterbium plumes. The EDX analysis revealed the relative concentration of Si:Yb = 1:2 and 1:2.25 in the distance of 4 and 8 cm from the target, respectively.

Two different types of nanoobjects were found in the sample synthetized at 800 °C: Clusters of nanoparticles (Fig. 2a) and nanorods (Fig. 2b). PEDT datasets collected from single nanoparticles (Fig. 2c) yielded a diffraction pattern with hexagonal unit cell with unit cell parameters: a = 6.6 Å, c = 4.1 Å. These parameters corresponded to the Yb_3Si_5 phase with the space group *P-62m* (Fig S3) [1]. The EDS elemental analysis resulted in Si:Yb = 64.4:35.7 and is close to theoretical values for Yb_3Si_5. The subsequent *ab initio* structure determination confirmed this structure.

Two distinct phases were identified in the nanorods. One phase was monoclinic with the unit cell parameters a = 9.1 Å, b = 9.0 Å, c = 14.6 Å, γ = 107°. This was identified in three nanorods. The result of the EDS analysis yielded Si:Yb = 63.0:37.0. The lattice parameters and chemical composition do not correspond to any phase in the binary system Yb-Si published so far. Unfortunately, the diffraction datasets were not suitable for the structure solution and refinement.

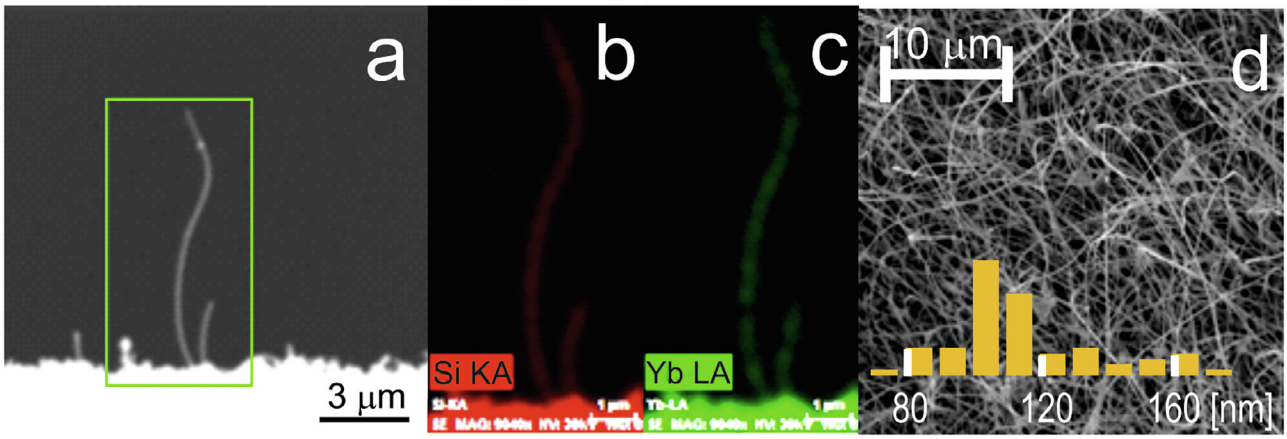

Fig. 1. a) SEM photo of NWs showing a selected area where EDX elemental mapping was performed and the elemental mapping of this area for b) silicon, c) ytterbium and d) SEM image of a NW deposit (1000 °C) with an indicated histogram of diameter distribution.

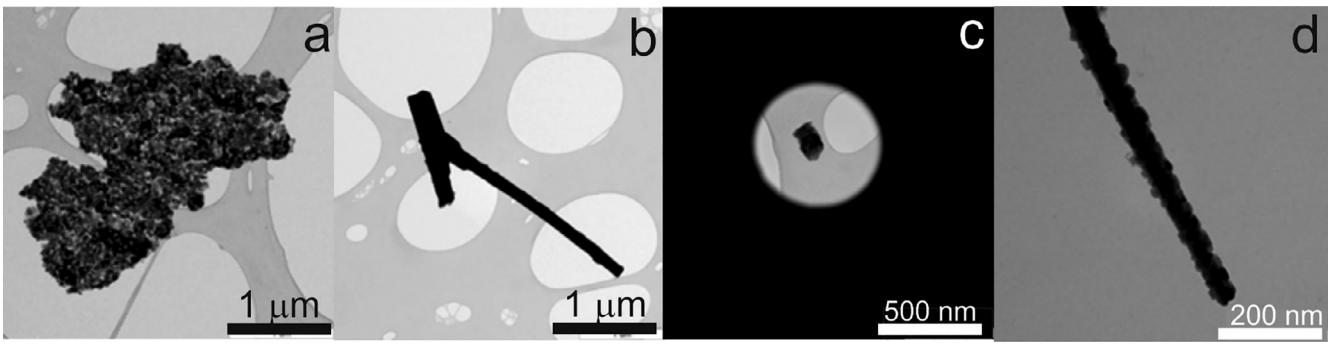

Fig. 2. High Resolution TEM bright-field (BF) images of a sample (800 °C) – (a) cluster of nanoparticles, (b) nanorods, (c) isolated nanoparticle – and BF image of a sample (1000 °C) – (d) nanorods.

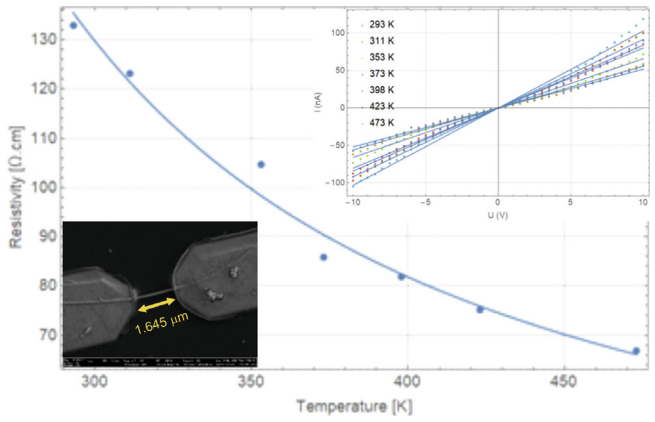

Fig. 3. The specific resistivity ρ of a NW from RT up to 473 K fitted with the Arrhenius plot. An inset photo down left shows SEM image of the studied NW and an inset upper right represents 2-point volt-ampere characteristics and resistivity linear fits at selected temperatures.

The second structure observed in the nanorods was the faced centered cubic (fcc) structure with lattice parameter a = 5.2 Å. This unit cell was not far from the parameters of pure Yb (a = 5.48 Å) [8] with the space group *Fm-3m*. The shorter lattice parameters might be the result of the partial substitution of Yb atoms by Si atoms. However, the EDS analysis – Si:Yb = 39.0:61.0 – indicated a much higher content of Si in that phase which is not in accordance with the equilibrium phase diagram Yb-Si. We note that the sample was prepared under non-equilibrium conditions.

The dominant morphology observed in the sample synthetized at 1000 °C were nanorods covered with nanoparticles (Fig. 2d). Electron diffraction patterns showed that the nanorods with composition Si:Yb = 43.6:56.4 were completely or almost completely amorphous. It was not possible to receive good diffraction data from the nanoparticles on the surface of nanorods. Fortunately, one isolated nanoparticle could be found and measured. It belonged to the same cubic phase as the one found and described in the previous sample, i.e. a fcc phase with a = 5.2 Å resembling pure Yb but with high Si contents (Si:Yb = 26.1:73.9).

Resistivity measurements were performed in the 2-point assembly, as shown in Fig. 3 (inset photo) from RT up to 473 K. The electrical resistance R was evaluated using the linear fit of the Ohm law [9]. The resistivity ρ in [Ω.cm] of a NW is related to the measured resistance R by the formula $\rho = R\frac{S}{d}$ where d is the length, $S = \pi\left(\frac{D}{2}\right)^2$the cross section and D the diameter of the NW. Here we know that $d = 1.645\mu$m and $D = 0.12\mu$m.

Since the resistivity ρ was significantly higher than the expected resistivity in metals (132.9 Ω.cm at RT) and it decreased with the increasing temperature T, as commonly observed in semiconductors, we evaluated the activation energy E_A from the Arrhenius plot $\rho = c.\exp(E_A/k_B{}^*T)$, where k_B is Boltzmann constant (Fig. 3). From the Arrhenius plot it follows that the NW was a doped semiconductor with activation energy 0.048 eV. The room temperature specific resistivity of the intrinsic bulk silicon was about 100 kΩ.cm [10]. The resistivity of a semiconductor decreases with the increasing temperature and it can be strongly reduced by many orders of magnitude in the presence of impurities. For example, the heavily doped silicon had the resistivity of about 1 Ω.cm which increased with temperature [11].

4. Conclusions

Using a laser as an instrument for material vaporization and an oven providing a heated zone for better relaxation of ablated species resulted in the synthesis of nanostructures partly of unknown structure. Both monoclinic and fcc structures of nanorods did not fit into the binary phase diagram Yb-Si. Moreover, the (almost) amorphous ytterbium silicide nanowires with high metal content possessed specific resistivity close to a heavily doped silicon. This way, the experimental set-up was found to be useful for the synthesis of unknown and advanced nanoscale alloys.

Acknowledgement

The support of the Academy of the Sciences of the Czech Republic (grant Strategy AV21 "Nanostructured materials for energy conversion") is gratefully acknowledged.

Conflict of interest

The authors declare that they have no conflict of interest.

Appendix A. Supplementary data

Supplementary data to this article can be found online at https://doi.org/10.1016/j.matlet.2019.03.032.

References

[1] A. Grytsiv, D. Katzorowski, A. Leithe-Jasper, V.H. Tran, A. Pikul, P. Rogl, M. Potel, H. Noel, M. Bohn, T. Velikanova, J. Solid State Chem. 163 (2002) 178–185.
[2] M.V. Kuzmin, M.A. Mitsev, A.M. Mukhuchev, Phys. Solid State 57 (2015) 2112–2116.
[3] J.W. Choi, M.C. Nguyen, A.H.T. Nguyen, S.Y. Han, J.Y. Kim, R. Choi, Nanosci. Nanotechnol. Lett. 9 (2017) 548–552.
[4] S. Tanulsip, Y. Ohishi, H. Muta, S. Yamanaka, A. Nishide, J. Hayakawa, K. Kurosaki, Phys. Status Solidi RRL (2017) 1700372.
[5] O. Janka, J.V. Zaikina, S.K. Bux, H. Tabatabaifar, H. Yang, N.D. Browning, S.M. Kauzlarich, J. Solid State Chem. 245 (2016) 152–159.
[6] L. Palatinus, PETS – Program for Analysis of Electron Diffraction Data, Institute of Physics of the AS CR, Prague, 2011, http://pets.fzu.cz/.
[7] V. Petricek, M. Dusek, L. Palatinus, Z. Krist. 229–5 (2014) 345–352.
[8] B.J. Beaudry, P.E. Palmer, J. Less Common Metals 34 (1974) 225–231.
[9] Y. Singh, Int. J. Mod. Phys.: Conference Series. 22 (2013) 745–756.
[10] S.M. Lindsay, Introduction to Nanoscience, Oxford University Press, Oxford, 2010.
[11] P.W. Chapman, O.N. Tufte, J.D. Zook, D. Long, J. Appl. Phys. 34 (1963) 3291–3295.